IET Radar, Sonar & Navigation

Research Article

IET Journals
The Institution of Engineering and Technology

Adaptive spectral processing algorithm for staggered signals in weather radars

ISSN 1751-8784
Received on 21st February 2020
Revised 1st June 2020
Accepted on 2nd June 2020
doi: 10.1049/iet-rsn.2020.0095
www.ietdl.org

Q1

Arturo Collado Rosell[1,2] ✉, *Juan Pablo Pascual*[1,2,3], *Javier Areta*[3,4]

[1]*Instutito Balseiro - Universidad Nacional de Cuyo, Av. Bustillo 9500, S.C. Bariloche, Argentina*
[2]*LIAT, Dto. de Ingeniería en Telecomunicaciones, GDTyPE, GAIyANN, CNEA, Av. Bustillo 9500, S.C. Bariloche, Argentina*
[3]*Consejo Nacional de Investigaciones Científicas y Técnicas (CONICET), Argentina*
[4]*Universidad Nacional de Río Negro, Anasagasti 1463, S.C. Bariloche, Argentina*
✉ *E-mail: arturo.collado@ib.edu.ar*

Abstract: A spectral algorithm for processing staggered-pulse repetition time (SPRT) signals in weather radar is introduced. It includes new approaches for ground clutter filter and hydrometeor spectral moments estimation. The algorithm uses ideas similar to GMAP but applied to non-uniform sampled signals. This work is focused on staggered sequences 2/3, but can be extended to other staggered sequences. Monte Carlo experiments were used to evaluate the performance of the spectral moments estimators for simulated weather signal, in scenarios with and without the presence of ground clutter. When clutter is present, a study using different clutter-to-signal ratios was carried out, showing that the method can deal with a wide range of situations and is appropriate for implementation in real scenarios. A comparison against GMAP-TD was performed, showing similar estimation results for both algorithms and a fivefold processing speed improvement for the proposed method. The performance was also validated using real weather data RMA-12 from a radar located in San Carlos de Bariloche, Argentina. The proposed algorithm has an easy implementation and is a good candidate for real-time implementations.

1 Introduction

In general, the weather radar returned signal can be modelled as the sum of contributions from meteorological targets, ground clutter – for low elevation angles – and noise. When the radar operates at uniform pulse repetition time (PRT), there is a trade-off between the maximum unambiguous range and the maximum unambiguous Doppler velocity, improving one of them implies worsening the other [1]. Several approaches have been proposed to deal with this issue [2]. One of the most used consists of transmitting a pulse sequence with the varying time interval between successive pulses, i.e. the radar uses alternately different PRTs. This radar operating mode, known as staggered-PRT (SPRT), allows estimating high unambiguous velocity without the unambiguous range degradation. Although there are different PRT combinations [3], a two-PRT system is often used, where the pulse interval alternates between PRTs T_1 and T_2 ($T_2 > T_1$). The unambiguous velocity for this scheme depends on $T_2 - T_1$ [2].

Ground clutter is produced by reflections from ground targets, like mountains, buildings, trees, among others. For low elevations angles, ground clutter obscures the precipitation signal and produces biased estimates of the spectral moments. Thus, its suppression is an important task for improving weather radar data quality. Clutter mitigation for SPRT signals is more challenging than in the uniform sampling case. Doppler tools as the discrete Fourier transform (DFT) cannot be used directly in the staggered data time sequence [4].

In the case of uniform PRT, a basic technique used to mitigate ground clutter consists of applying a notch filter around zero Doppler velocity [5]. This approach has been adapted to SPRT [6]; the scheme uses two filters to mitigate the ground clutter. The input time series with non-uniformly spaced samples are divided into two time series with uniformly spaced samples and then processed using one of the two filters for each uniform signal. To design the filters, they use equirriple or window methods [6], obtaining better performance with the windows design. If the precipitation Doppler velocity is near zero, these notch filters have the disadvantage of filtering the precipitation signal, leading to biased spectral moments estimates.

Advanced filtering methods have been proposed for clutter mitigation and spectral moments estimation using SPRT signals [4, 7–14]. In general, they consist of adaptive strategies that interpolate the removed spectral components.

Gaussian model adaptive processing (GMAP) is, probably, the most common clutter adaptive filter [15]. It replaced the bank of elliptic filters of the Weather Surveillance Radar-1988 Doppler (WSR-88D) [16] and its current implementation was complemented by the clutter mitigation decision (CMD) algorithm which controls its application [17, 18]. GMAP is a spectral domain method that filters ground clutter using a clutter mask and attempts to recover the removed precipitation components considering a Gaussian shape for the power spectral density (PSD) of the meteorological target. GMAP was developed initially for uniform sampling signals, but recently it had been adapted to process SPRT signals [7–9]. It is worth pointing out that all of these approaches generate a uniform time sequence from the SPRT sequence to apply GMAP in its standard form. In [8], the authors separate the SPRT signal into two uniformly time sequences with a greater time period, $T_1 + T_2$, and then process each of them using GMAP for uniform-PRT. After GMAP, they disambiguate the mean velocity. The accuracy of the moment estimate is low as a consequence of the Doppler interval reduction. In [9], the authors rebuild the uniform sampled PSD of the signal using a technique for non-uniform sampling digital spectrum reconstruction [19]. After the PSD reconstruction, they use the standard form of GMAP for clutter filter and spectral moments estimate. This method suffers from the limitation that the unambiguous velocity depends on $(T_1 + T_2)/2$.

Among the algorithms implemented in the time domain, we can mention the parametric time-domain method (PTDM) [12], which uses the maximum likelihood estimator to obtain the spectral moments of ground clutter, precipitation and noise level, assuming that the multivariate probability density function of the received complex voltage has Gaussian shape. Also, they use a Gaussian model for the observed Doppler spectrum of clutter and precipitation. The main drawback of the method is its high computational cost, which prevents it from being implemented for real-time operation [13]. It is also difficult to assure the

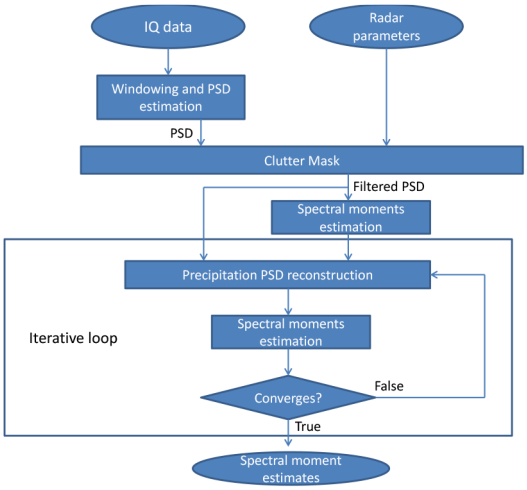

Fig. 1 *ASPASS flowchart*

optimisation problem convergence for the reduced number of samples available in practice for each coherent processing interval. Another algorithm is the so-called Gaussian model adaptive processing in the time domain [13] (GMAP-TD). This is a method that consists of applying a filter to the signal autocorrelation and recovering the precipitation signal component through an iterative procedure based on fitting a Gaussian autocorrelation precipitation model. GMAP-TD can be implemented for uniform and staggered PRT signals, but is also computationally intensive. Unlike GMAP, to our knowledge, PTDM and GMAP-TD have not had practical implementations in any operational weather radar.

For methods applied in the spectrum domain, we can mention the spectral algorithm for the clutter harmonics identification (SACHI) algorithm [4, 10, 11], in which time signal is zero interpolated in order to create an artificial uniform sampled signal. The authors introduced a new method to filter ground clutter and use a deconvolution process for precipitation signal spectrum reconstruction. The original SACHI algorithm [4, 10] lacked the flexibility to adapt to the clutter environment in real-time. For that reason, a table with clutter widths was built in order to account for dynamic changes of clutter characteristics, called SACHI-table [20]. A robust method for staggered spectral width clutter estimation is found in the algorithm SACHI-GMAP [7, 11], which uses GMAP for clutter width estimation. Other important algorithm is the clutter environment analysis using adaptive processing (CLEAN-AP) [16], which was extended to work with SPRT signals. At the core, this algorithm uses the autocorrelation spectral density (ASD) introduced in [14] as an extension of the classical periodogram-based power spectral density (PSD). ASD includes spectral phase information, which provides a better tool for the identification of narrow-band signals, such as those typical of ground clutter.

In this work, we present an adaptive method that uses processing steps similar to GMAP, for processing staggered sequences, termed adaptive spectral processing algorithm for staggered signals (ASPASSs). It is a novel spectral algorithm for clutter mitigation and precipitation spectral moments estimation. We assume the common hypotheses for this kind of problem, i.e. Gaussian-shaped clutter and precipitation PSDs, with precipitation spectra significantly wider than clutter spectra [1, 21–23]. Even when ASPASS's approach is similar to GMAP, it differs from the existing versions of GMAP for SPRT sequences. It does not apply GMAP in its standard form after signal manipulation as in [7–9], instead, ASPASS processes the SPRT spectrum obtained by transforming the zero interpolated staggered sequence, following GMAP's logic of finding a clutter mask, removing clutter and iteratively reconstructing the weather spectra while performing moments estimation. The clutter mask and the reconstruction stage consider the spectral replicas resulting from the zero interpolation, and the moment estimators have been modified for this situation. The main advantage of the proposed algorithm is computational load reduction while providing accurate estimators.

The paper is organised as follows. The description of the algorithm is presented in Section 2. Numerical simulations using synthetic data are discussed in Sections 3. Real weather radar data from radar RMA-12 is processed in Section 4. Finally, Section 5 presents conclusions.

2 ASPASS description

ASPASS operates on the spectrum of the zero interpolated staggered sequence, applying a mask to remove the clutter – and possibly signal – components. It then iteratively reconstructs the weather signal by adjusting the signal model to the weather samples remaining. In this process, the spectral moments are estimated, until the reconstruction process converges. The following are the main steps of the algorithm, also described graphically in Fig. 1, the rest of the section contains a detailed description of each step.

- Zero interpolation in order to have a uniform sampling time T_u, windowing and PSD estimation using periodogram [24].
- Ground clutter power estimation, if present.
- Determination of clutter points and removal of clutter points using a mask. If no clutter is present, the mask is not applied.
- Inverse Fourier transform of PSD and estimation of power, mean velocity and spectral width of precipitation. Reconstruction of PSD using the last estimates and the PSD model consisting of five Gaussian functions. Replace clutter points in the PSD. Repeat this process until the difference between two consecutive velocity and power estimates are less than $0.005v_{max}$ and 0.1 dB, respectively.

2.1 Zero interpolation, windowing and PSD estimation

In general, the staggered PRT technique uses two different pulse spacings T_1 and T_2 alternately [2]. These pulse spacings can be selected such that they are integer multiples of some basic PRT T_u, $T_1 = n_1 T_u$ and $T_2 = n_2 T_u$. In this work, we focus on the case where $n_1 = 2$ and $n_2 = 3$ known as staggered 2/3. This PRTs ratio is the most used in weather radar [25], because it achieves the best compromise between the maximum unambiguous velocity and the quality of the spectral moments estimates [2]. In staggered PRT sequences, the signal spectrum cannot be obtained using the standard DFT, which is defined for uniformly sampled sequences. For that reason, we interpolate the time series data with zeros in order to obtain a uniform sequence with a sampling rate T_u (the zeros are added between the staggered samples). The PSD of this new data is estimated using the periodogram [24]. It contains replicas of clutter and weather echoes present at certain velocities. These velocities depend on the staggered PRT relation (n_1/n_2). Windowing is needed before PSD estimation in order to attenuate the sidelobes effect. The window used depends on the clutter-to-

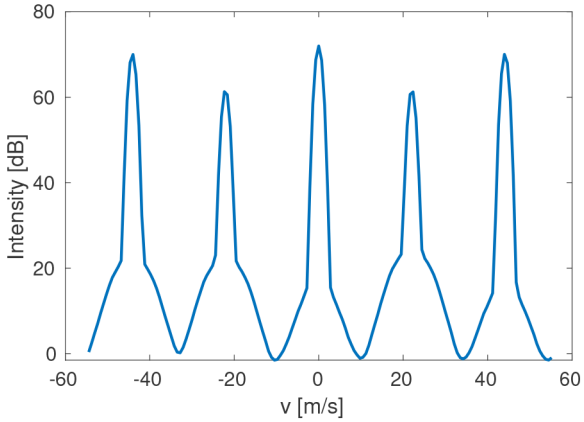

Fig. 2 *PSD after zero interpolation of simulated data containing clutter, precipitation and noise*

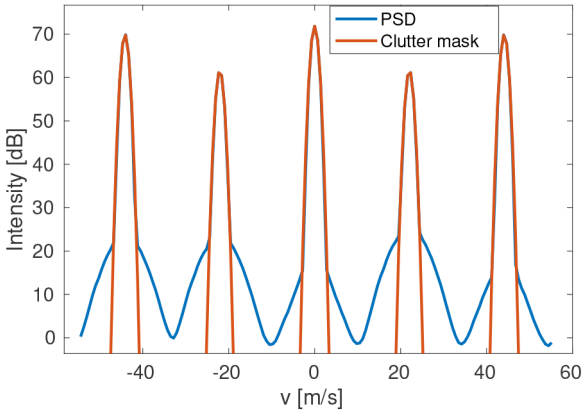

Fig. 3 *PSD and clutter mask for the typical staggered case*

signal ratio (CSR). We used Kaiser windows since one parameter allows for a large range of sidelobe level attenuation [26].

For ground clutter, the main replica is located at zero velocity and the others at $\pm(2kv_{\max}/(n_1+n_2))$ [13], where $k = 1, 2, \ldots,$ Integer$[(n_1+n_2)/2]$ and $v_{\max} = \lambda/4T_u$ is the maximum unambiguous velocity, λ is the wavelength. For the weather spectrum, the replicas are separated $2v_{\max}/(n_1+n_2)$ from each other as clutter replicas, but the main replica is at v_p. Fig. 2 shows the PSD of a 2/3 staggered sequence after zero interpolation of simulated ground clutter, precipitation and noise. The simulation parameters were $F_c = 3$ GHz (carrier frequency), CSR = 40 dB, $N = 64$ (number of samples), $T_1 = 1$ ms, $T_2 = 1.5$ ms, SNR = 20 dB (signal-to-noise ratio), $I = 1000$ (number of realisations to estimate the PSD), $v_p = 0.4v_{\max}$ (precipitation mean velocity) and $\sigma_p = 3$ m/s (precipitation spectral width). This simulation is denoted as a *typical staggered case* in the remaining of this paper, and will help to visualise the PSD for the different steps of the algorithm. Synthetic data used through this paper was generated following the ideas presented in [27].

2.2 Ground clutter filtering

For staggered sequence 2/3, the five clutter replicas are located at 0 m/s, $\pm 0.4v_{\max}$ and $\pm 0.8v_{\max}$. To filter the clutter, we construct a mask and select the five regions in which the clutter is present. The mask is modelled as the sum of five Gaussian functions. Fig. 3 shows the signal PSD and the clutter mask for the *typical staggered case*. The mask equation results

$$Mask(v) = \frac{\hat{p}_c}{\sqrt{2\pi}\sigma_c} e^{-(v)^2/2\sigma_c^2} + \frac{0.095\hat{p}_c}{\sqrt{2\pi}\sigma_c} e^{-(v\pm 0.4v_{\max})^2/2\sigma_c^2} + \frac{0.655\hat{p}_c}{\sqrt{2\pi}\sigma_c} e^{-(v\pm 0.8v_{\max})^2/2\sigma_c^2}, \quad (1)$$

where $\hat{p}_c$ is the estimated power of the clutter replica at zero velocity. The coefficients 0.095 and 0.655 were obtained numerically using Monte Carlo simulation; see Section 8.1 of the Appendix. The actual clutter power is estimated as $2.5\hat{p}_c$.

2.2.1 Clutter power: To build the clutter mask, we need to estimate $\hat{P}_c$ and σ_c. The last parameter is estimated as in [28] but using a Kaiser window. The authors in [28] use the fact that the observed PSD after windowing is the convolution of the asymptotic PSD and the window energy spectral density (ESD). They calculate the observed clutter σ_c width as $\sigma_c = \sqrt{\sigma_t^2 + \sigma_w^2}$, where σ_t is the asymptotic clutter width, calculated using physical antenna parameters like the scan rate, antenna diameter, wavelength and the 3-dB one-way power pattern beamwidth [1], σ_w is the spectrum width of the ESD and it is obtained as the result of the Gaussian fit. σ_w has been tabulated for different Kaiser windows and samples number N.

In order to obtain $\hat{P}_c$, we use the three central points of the main clutter replica, as in GMAP [15]. This clutter mask is dynamically calculated, so the algorithm can be used in real scenarios. Fig. 4 shows the PSD after clutter mitigation for the *typical staggered case*.

2.3 Precipitation spectral moments estimation

If the weather signal only contains precipitation with power P_p, mean velocity v_p and spectrum width σ_p, obtained with staggered sequence 2/3, after zero interpolation the precipitation PSD consist of the sum of five Gaussian functions centred at v_p, $v_p \pm 0.4v_{\max}$ and $v_p \pm 0.8v_{\max}$

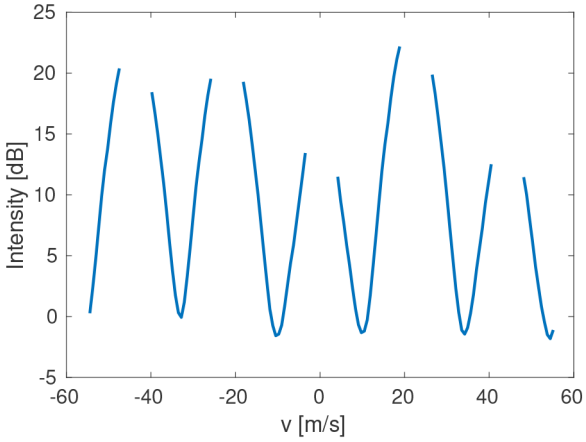

Fig. 4 *PSD after clutter filter for the typical staggered case*

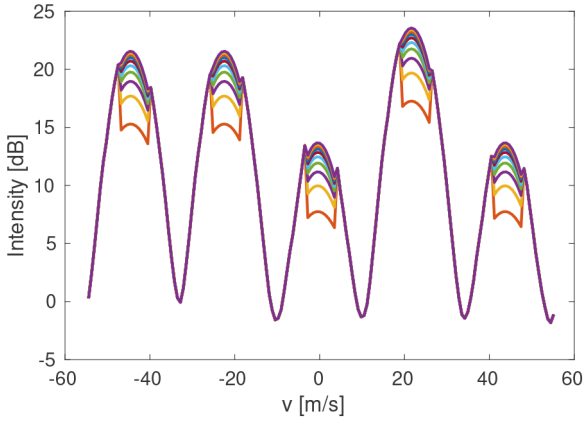

Fig. 5 *Precipitation PSD reconstruction for the typical staggered case*

$$S_p(v) = \frac{\hat{p}_p}{\sqrt{2\pi}\sigma_p} e^{-(v - v_p)^2/2\sigma_p^2} + \frac{0.095\hat{p}_p}{\sqrt{2\pi}\sigma_p} e^{-(v - v_p \pm 0.4v_{\max})^2/2\sigma_p^2} + \frac{0.655\hat{p}_p}{\sqrt{2\pi}\sigma_p} e^{-(v - v_p \pm 0.8v_{\max})^2/2\sigma_p^2}, \quad (2)$$

where $\hat{p}_p$ is the power of the Gaussian at v_p. This model is a good approximation for the range of spectrum widths in which the overlap of replicas can be ignored. The autocorrelation function $R_p(\tau)$ is obtained by taking the inverse Fourier transform of (2)

$$R_p(\tau) = \hat{p}_p e^{-j4\pi v_p \tau/\lambda} e^{-8\pi^2\sigma_p^2\tau^2/\lambda^2} \left(1 + 0.095\, e^{\pm j4\pi 0.4 v_{\max}\tau/\lambda} + 0.655\, e^{\pm j4\pi 0.8 v_{\max}\tau/\lambda}\right). \quad (3)$$

This expression can be simplified as

$$R_p(\tau) = \hat{p}_p e^{-j4\pi v_p \tau/\lambda} e^{-8\pi^2\sigma_p^2\tau^2/\lambda^2} \left[1 + 2\times 0.095\cos\left(\frac{4\pi 0.4 v_{\max}\tau}{\lambda}\right) + 2\times 0.655\cos\left(\frac{4\pi 0.8 v_{\max}\tau}{\lambda}\right)\right]. \quad (4)$$

It is important to note that $R_p(\tau)$ is not the same as the autocorrelation of the staggered signal without zero interpolation, $R(\tau)$. There is a strong relationship between R and R_p coefficients, they differ only by a scale factor for some lags. An analogue methodology to pulse pair processing (PPP) [1], which uses the first lags of the function $R_p(\tau)$ can be applied to estimate the precipitation power, mean velocity and spectrum width

$$\hat{P}_p = R_p(0) = 2.5\hat{p}_p \quad (5)$$

$$\hat{v}_p = \frac{\lambda}{4\pi T_u}\text{angle}\left(\frac{R_p(T_1)}{R_p(T_2)}\right) \quad (6)$$

$$\hat{\sigma}_p = \frac{\lambda}{2\sqrt{2}\pi T_1}\sqrt{Ln\left|\frac{R_p(0)}{2R_p(T_1)}\right|}. \quad (7)$$

Note that the expression of the velocity estimator is similar to the classical PPP for staggered sequences (PPP-S) [2], since the phases of $R(T_1)$ and $R(T_2)$ are equal to the phases of $R_p(T_1)$ and $R_p(T_2)$, respectively. For this reason, we denote the velocity estimator as equivalent to PPP-S (EPPP-S) estimator. EPPP-S, like PPP-S, is computed as the quotient of two estimators what generally implies that it has a high variance [10]. In order to improve the estimator precision, it is possible to use the dealising method (DA) [10] in terms of the autocorrelation function $R_p(\tau)$. It consists on the computation of two velocity estimates, $\hat{v}_1$ from $R_p(T_1)$ and $\hat{v}_2$ from $R_p(T_2)$, which, in general, are aliased. Then, $\hat{v}_2$ is only used to disambiguate the velocity estimate obtained using $R_p(T_1)$ that has a lower variance. The estimators EPPP-S and DA are compared in Section 3.1 to appreciate the difference in their performance.

2.4 Precipitation PSD reconstruction and noise consideration

After clutter filtering some, overlapping, precipitation spectrum samples are eliminated too. The truncated PSD is antitransformed to obtain $R_P(\tau)$. The parameters $\hat{p}_p$, v_p and σ_p are obtained using the proposed estimators. Then, the missing PSD samples are filled using (2). This process is repeated until the computed power does not change by >0.1 dB and the mean velocity does not change by >0.005 of $v_{\max}$ [15]. Fig. 5 shows the reconstruction process of the precipitation PSD for the *typical staggered case*.

Noise is present in all real systems and is herein modelled as white [1]. If the weather target is not too far from the radar, the SNR is normally >20 dB. Thus an SNR of 20 dB is used in all the simulations in this work. This is reasonable since clutter is present at close ranges, generally in the first 20 km where the previous consideration is valid. Since the spectrum floor is dominated by clutter and precipitation spectrum overlapping replicas, the noise effect was not taken into account in ASPASS estimators. For the case of smaller SNR the noise level should be taken into account, resulting in a degradation of the ASPASS estimates.

3 Numerical simulations

Monte Carlo simulations were conducted in order to verify the correct operation of the algorithm. The section is splitted in four subsections. In the first one, the performance of the estimators presented in Section 2.3 is studied using different σ_p values when ground clutter is not present. The second subsection presents ASPASS performance when clutter is present. A comparison against GMAP-TD is done to assess performance. The third subsection presents a computational complexity analysis. The last subsection shows the error analysis for different CSR values.

3.1 ASPASS performance without ground clutter

In this subsection, we simulate weather radar signals without clutter, only precipitation and noise. The purpose is to compare the performance obtained using three different velocity estimators, EPPP-S (6), DA and the classical PPP-S, and the performance of the PPP-S spectral width estimator with the one proposed (7). The precipitation signal was simulated having a Gaussian PSD, and white additive noise. The simulation parameters are shown in Table 1, 10,000 Monte Carlo realisation where used for each spectral width in the range of 1–8 m/s.

Fig. 6 shows the bias and standard deviation of mean velocity and spectrum width for the aforementioned estimators. In the case of PPP-S, the spectrum width estimator used is based on $\log[R(0)/R(T_1)]$. PPP-S results consider the raw data stream, no window, while EPPP-S and DA use a Kaiser window with $\alpha = 6$ because for these methods the autocorrelation is estimated by means of the PSD. The usage of windows other than the

Table 1 Simulation input parameters. Depend on the simulation type, some parameters are used or not

Parameter	Value
F_c, GHz	3
CSR, dB	0, 40
SNR, dB	20
σ_t, m/s	0.3
σ_p, m/s	[1, 2, 3, 4, 5, 6, 7, 8]
v_p, m/s	0, …, v_{max}
N, samples	64
T_u, ms	0.5
T_1/T_2	2/3

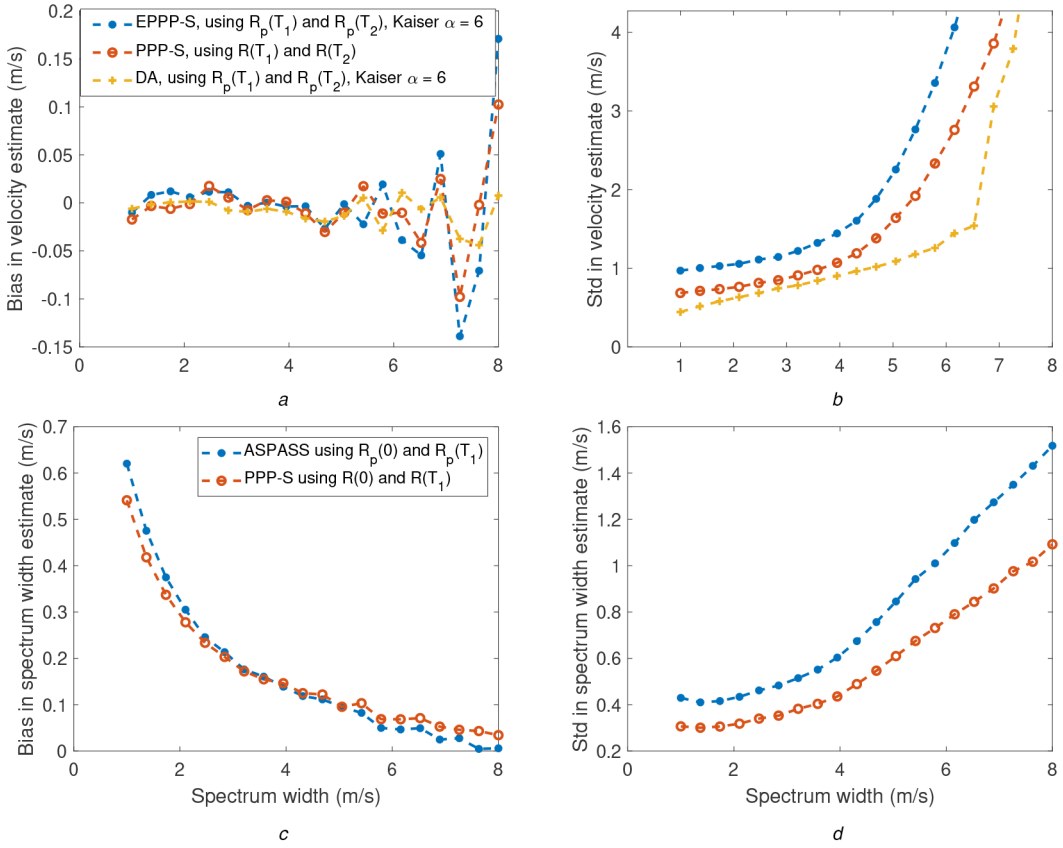

Fig. 6 *(a), (b) Velocity error analysis for EPPP-S, PPP-S and DA using staggered 2/3 simulated weather signal without clutter*
(a) Bias and ***(b)*** Standard deviation. (c), (d) Spectrum width error analysis for ASPASS and PPP-S. ***(c)*** Bias and ***(d)*** Standard deviation

rectangular worsens the estimation results. Even though there is no clutter present we want to consider a worst case scenario. From Fig. 6 we can conclude that all the methods present similar biases for velocity and spectrum width. The standard deviation in velocity is noticeably smaller for DA, as expected. Finally, the standard deviation in the spectrum width is smaller for PPP-S due to the windowing effect. In the case of no window, (6) and (7) have identical performance to PPP-S since these equations boil down to PPP-S equations.

DA will be used for velocity estimation in ASPASS, instead of EPPP-S, given its lower variance and extended operation range in terms of weather spectrum width, providing good estimates up to 7 m/s. For wider spectrum the Gaussian replicas considerably overlap, worsening the estimation independently of the estimator used.

3.2 ASPASS performance when ground clutter is present

As a second step for performance evaluation of ASPASS we simulate weather radar signal with clutter. The simulation parameters are in Table 1, with CSR = 40 dB. For each v_p and σ_p, 1000 Monte Carlo realisations were used to evaluate estimation performance.

Fig. 7 shows the velocity error analysis. Three spectrum width regions, can be defined. For small spectrum widths, the bias and standard deviation at velocities 0 m/s, $\pm 0.4 v_{max}$ and $\pm 0.8 v_{max}$ are big, because when clutter is filtered considerable precipitation power is filtered too, biasing the first velocity estimate. This affects the convergence of the reconstruction process. For spectrum widths between 3 and 5 m/s, the bias and standard deviation are the smallest, the filtered precipitation spectrum samples do not prevent the algorithm from finding a good initial velocity estimate, obtaining a properly reconstructed PSD. For large spectrum widths the PSD gets distorted due to overlapping, affecting the estimations.

Fig. 8 shows the spectrum width error analysis. We can define the same three regions as in the velocity analysis. The performance when the spectrum width is around 1 m/s is the worst, for the same reason as the previous case. For $3 <= \sigma_p <= 5$, the performance improves, again due to having more precipitation spectrum samples for reconstruction. When spectrum width increases above 5 m/s, the bias stays around cero, but the standard deviation increases, due to PSD overlapping. It is worth mentioning that in all cases, the bias and standard deviation values are in the same order.

Fig. 9 shows the power error analysis. The same three regions can be observed. In the bias case, only the first region is noticeably

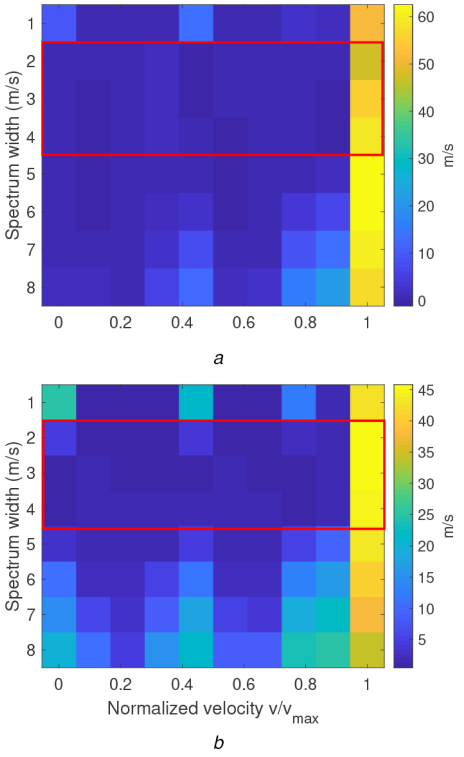

Fig. 7 *Velocity error analysis for ASPASS using staggered 2/3 simulated weather signal with CSR = 40 dB*
(a) Bias, and ***(b)*** Standard deviation

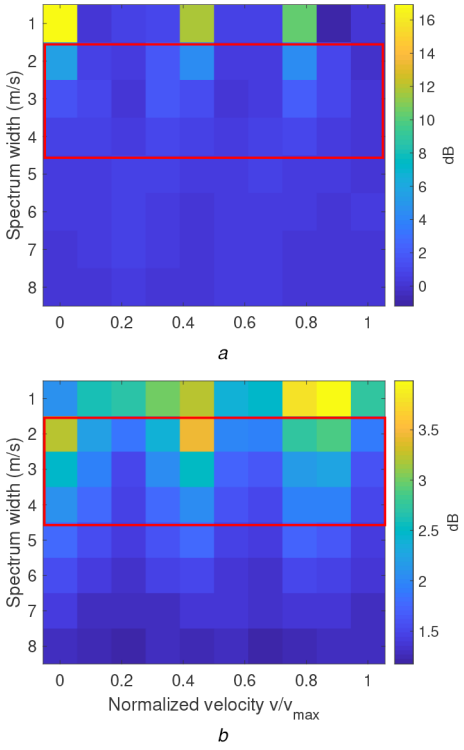

Fig. 9 *Power error analysis for ASPASS using staggered 2/3 simulated weather signal with CSR = 40 dB*
(a) Bias, and ***(b)*** Standard deviation

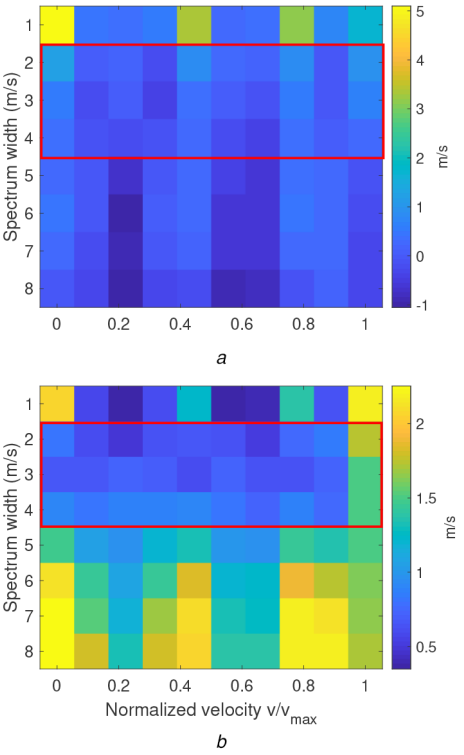

Fig. 8 *Spectrum width error analysis for ASPASS using staggered 2/3 simulated weather signal with CSR = 40 dB*
(a) Bias, and ***(b)*** Standard deviation

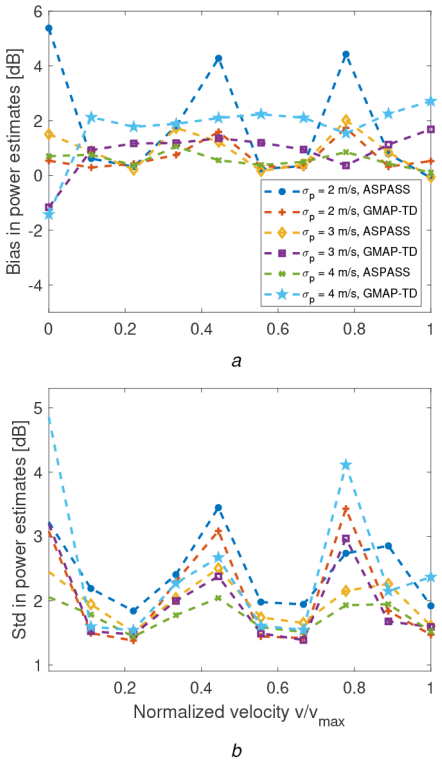

Fig. 10 *Power error analysis for ASPASS and GMAP-TD using staggered 2/3 simulated weather signal with CSR = 40 dB*
(a) Bias, and ***(b)*** Standard deviation

worst and improves as the spectral width increases. The same behaviour can be observed for the standard deviation, showing that for power estimation the effect of the overlapping replicas does not affect as in the previous cases.

We compared ASPASS against the staggered version of GMAP-TD. Figs. 10–12 show the bias and the standard deviation of the power, the velocity and the spectral width estimates as a function of the velocity, respectively, for both methods considering spectrum widths of 2, 3 and 4 m/s. For ASPASS, these plots correspond to the boxed regions in Figs. 7–9.

In the case of power estimates, ASPASS shows large bias and standard deviation at velocities 0 m/s, $\pm 0.4 v_{max}$ and $\pm 0.8 v_{max}$ for the case of narrow spectral width, $\sigma_p = 2$ m/s. When centred around the clutter replicas, this narrow signal is heavily affected by the clutter mask, which removes considerable precipitation power, biasing the first spectral moments estimates. For spectrum widths 3

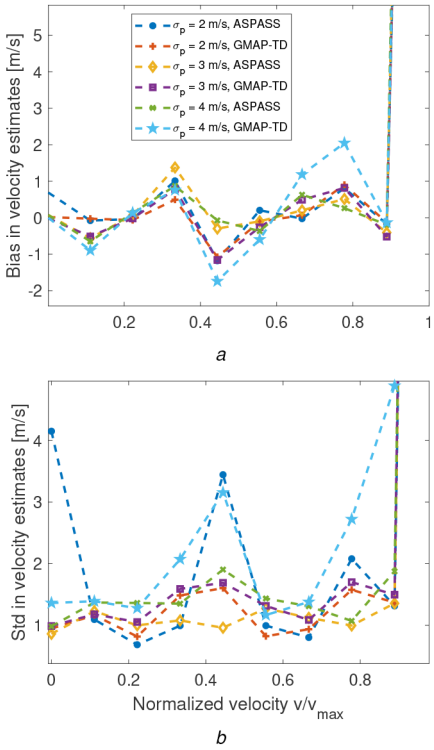

Fig. 11 *Velocity error analysis for ASPASS and GMAP-TD using staggered 2/3 simulated weather signal with CSR = 40 dB*
(a) Bias, and ***(b)*** Standard deviation

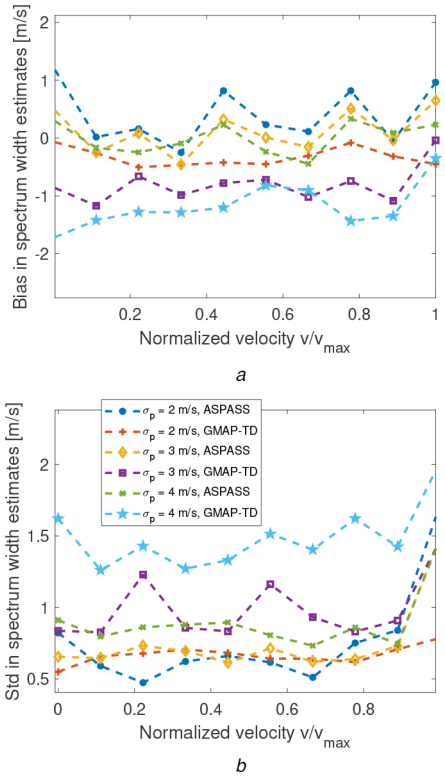

Fig. 12 *Spectrum width error analysis for ASPASS and GMAP-TD using staggered 2/3 simulated weather signal with CSR = 40 dB*
(a) Bias, and ***(b)*** Standard deviation

and 4 m/s ASPASS shows good performance, since the remaining precipitation power after clutter elimination is enough to make a good initial estimate. GMAP-TD obtains better power estimates for lower spectral widths than for larger widths. The reason can be traced to the overestimation of the noise floor. This estimate is used to construct the clutter filter, and is obtained in the spectrum domain where the replicas add to the noise floor resulting in an

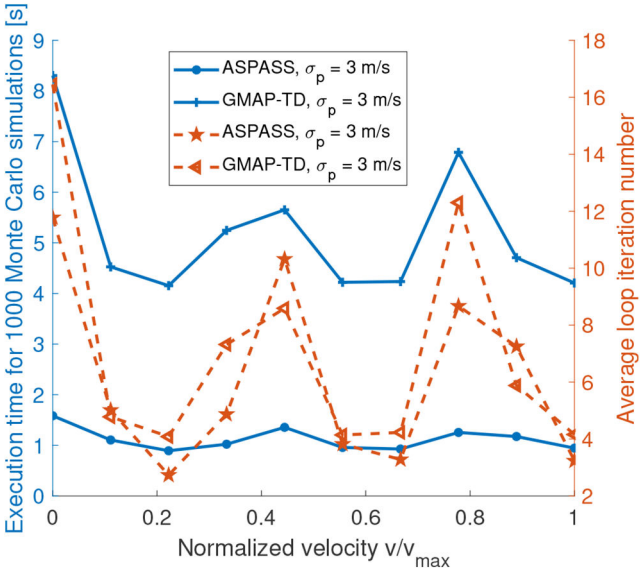

Fig. 13 *Execution time and the average number of iterations required to converge for ASPASS and GMAP-TD*

increasing over estimation, the wider the weather spectra. In general, both algorithms have power estimates degradation at the velocities where there are clutter replicas.

For velocity estimates, ASPASS again shows degradation at velocities 0 m/s, $\pm 0.4 v_{max}$ and $\pm 0.8 v_{max}$ for the case $\sigma_p = 2$ m/s. This degradation can be accounted for the same reason as in the case of power estimates. Similarly GMAP-TD shows good performance for lower spectrum widths, as the spectral width increased the performance degrades due to the erroneous noise floor estimation. In both algorithms, there is degradation at the velocities where there are clutter replicas.

The spectrum width error analysis shows good results for both algorithms, with slighter better quality in the case of ASPASS. The estimates degradation at velocities 0 m/s, $\pm 0.4 v_{max}$ and $\pm 0.8 v_{max}$ is not as noticeable as in the other cases, for both algorithms. Again GMAP-TD shows an appreciable degradation for $\sigma_p = 4$ m/s due to poor noise floor estimation.

3.3 Computational complexity of ASPASS

In this subsection, we present a computational complexity analysis of ASPASS and GMAP-TD, under a well-defined simulation scenario. Given that the algorithms are iterative, it is not possible to calculate exactly the number of operations required. Average runtime and average loop iteration number are chosen as the metrics to analyse complexity. The simulation consists of 1000 Monte Carlo experiments for each v_p, with the parameters listed in Table 1, considering only $\sigma_p = 3$ m/s, and these were run over the same platform using a PC with Intel core i3 8100 (3.6 GHz) processor and 16 GB of RAM.

Fig. 13 shows average execution time and average number of iterations until convergence for both algorithms. Even when they take a similar average number of iterations to converge, ASPASS is approximately five time faster than GMAP-TD, for the entire velocity range. This is a consequence of the number of operations that ASPASS requires at its most intensive step, i.e. the FFT, which is $O(M\log(M))$, where $M = 2.5N$, while GMAP-TD performs matrix multiplications, which are $O(N^2)$, and a matrix inversion which is $O(N^3)$. Note that the overlapping effect of the weather spectra with clutter replicas at velocities 0 m/s, $0.4 v_{max}$ and $0.8 v_{max}$ is again evident. In this case, through the increase of the iteration number required to converge in both methods.

3.4 ASPASS performance using different CSR

In this section, we study, which window to use depending on the CSR, since when the CSR increases, a more aggressive window is needed to reduce sidelobe effects. This in turn implies spectrum

Table 2 Simulation input parameters to evaluate ASPASS performance for different CSR

Parameter	Value
F_c, GHz	3
CSR, dB	0–70
SNR, dB	20
σ_t, m/s	0.3
σ_p, m/s	4
v_p, m/s	$0.4v_{max}$, $0.6v_{max}$
N, samples	64
T_u, ms	0.5
T_1/T_2	2/3

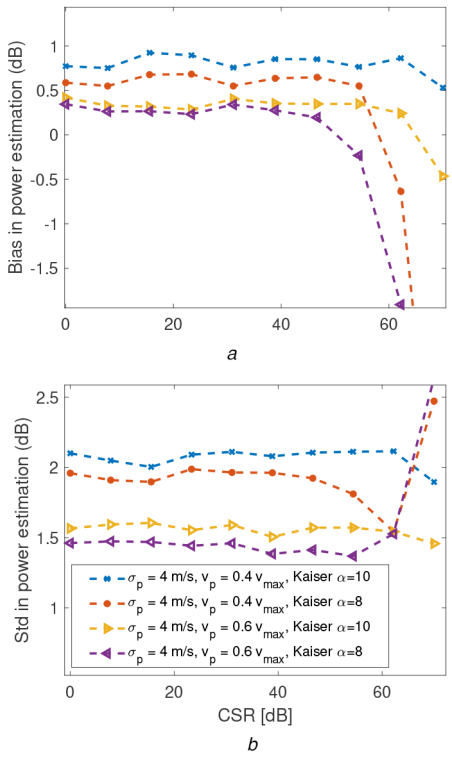

Fig. 14 *ASPASS power error analysis for different CSR*
(a) Bias, and ***(b)*** Standard deviation. Two Kaiser windows with $\alpha = 10$ and $\alpha = 8$ were used

broadening. To evaluate the performance of ASPASS for different CSR, 1000 Monte Carlo realisations were used. Simulations parameters are shown in Table 2. The two velocities were selected in order to see how the ASPASS performance changes when there is and there is not strong superposition between clutter and precipitation DEP. Figs. 14*a*, 15*a* and 16*a* show the bias and Figs. 14*b*, 15*b* and 16*b* show the standard deviation of the precipitation power, mean velocity and spectrum width, respectively. In order to compare the performance, two Kaiser windows with $\alpha = 10$ and $\alpha = 8$ were used. For CSR smaller than 50 dB, the less aggressive window performs slightly better in all cases. The performance differences can be accounted by the effect of the spectrum broadening. For CSR larger than 50 dB, the sidelobe level of the window with $\alpha = 8$, about 57 dB, becomes appreciable and degrades performance. The more aggressive window, in turn, keeps performance to a reasonable level.

In the case of power estimation, the behaviour for CSR around 60 dB is counter intuitive as the standard deviation diminishes rather than increasing. The reason is the initial underestimation of the power level turns into an overestimation for high CSR. Around 60 dB the bias errors cancel out explaining the performance improvement.

In practice, we suggest using different windows for different CSR. When there is no clutter use a rectangular window. For

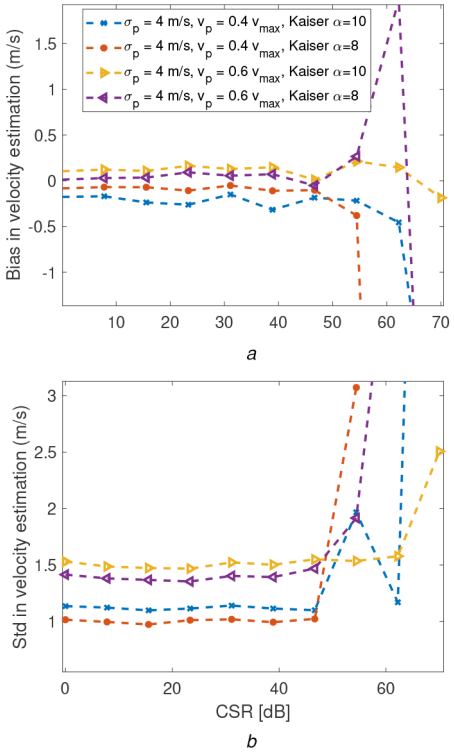

Fig. 15 *ASPASS velocity error analysis for different CSR*
(a) Bias, and ***(b)*** Standard deviation. Two Kaiser windows with $\alpha = 10$ and $\alpha = 8$ were used

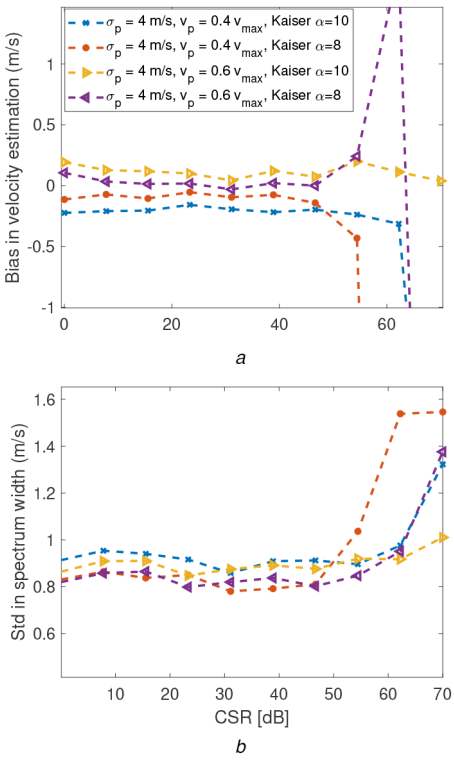

Fig. 16 *ASPASS spectral width error analysis for different CSR*
(a) Bias, and ***(b)*** Standard deviation. Two Kaiser windows with $\alpha = 10$ and $\alpha = 8$ were used

intermediate CSR (5–30 dB) use a Kaiser window with $\alpha = 6$, which has a sidelobe rejection close to 43 dB. For strong CSR (30–50 dB) use a Kaiser window with $\alpha = 8$. In the case of having larger CSR, a more aggressive Kaiser window can be used having reasonable performance too.

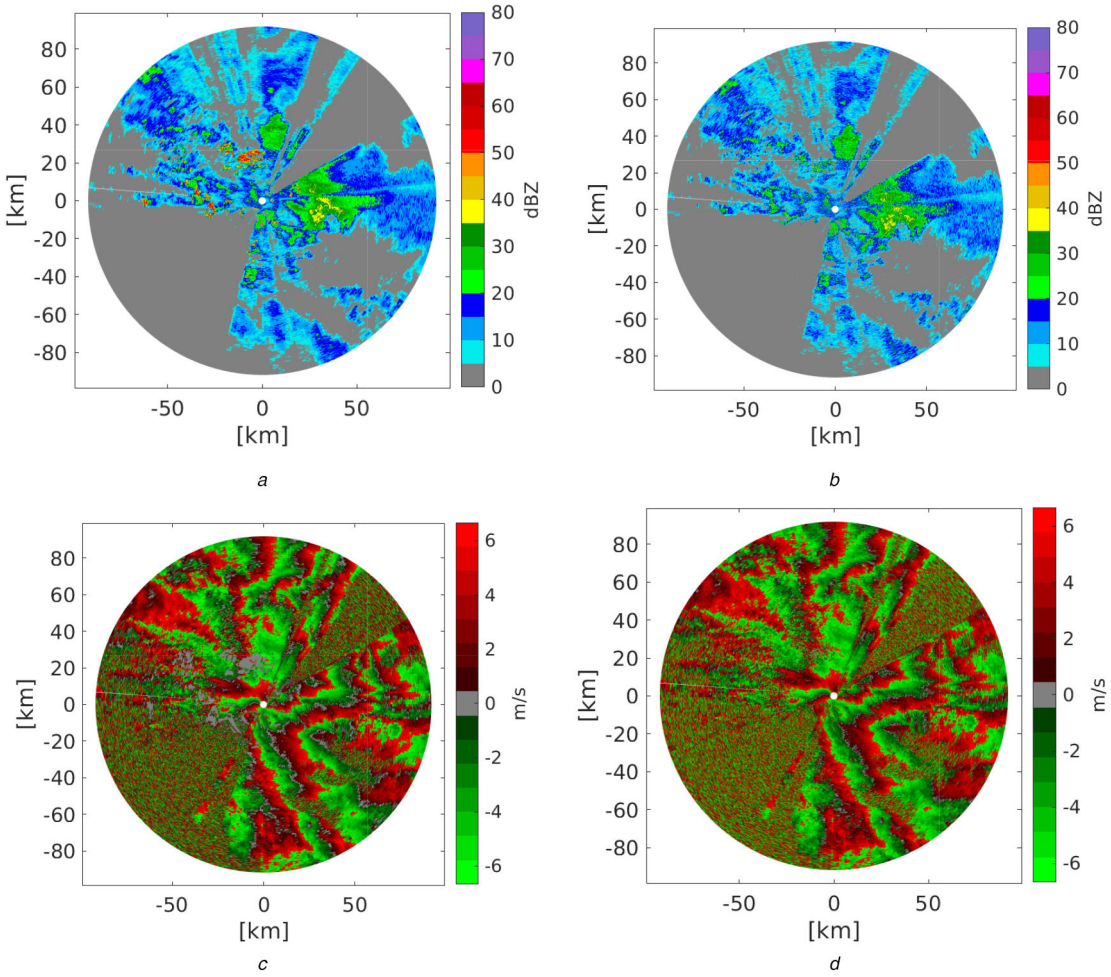

Fig. 17 *PPI plots show the performance of PPP and GMAP on RMA-12 measurements*
(a) Reflectivity from data collected with RMA-12, ***(b)*** Reflectivity obtained after GMAP processing, ***(c)*** Velocity before ground clutter filter using PPP, ***(d)*** Velocity using GMAP

4 Application to RMA-12 data

In this section, we present results when using the proposed algorithm on real weather radar data. The measurements were collected by the RMA-12 Argentinian weather radar, located in San Carlos de Bariloche city. The RMA-12 is a C-band polarimetric radar, designed and developed by the company INVAP. Specifically, the used data were recorded on 1 June 2015, under intense rain meteorological conditions.

The show results correspond to two complete sweeps of the horizontal polarisation (HH) at 2.3° elevation angle, ensuring that there were precipitation and clutter components present. The first sweep uses a staggered-PRT 2/3, with $T_1 = 0.8$ ms and $T_2 = 1.2$ ms, resulting an unambiguous velocity of 33.25 m/s. The second sweep corresponds to a uniform PRT sequence, with $T = 2$ ms resulting an unambiguous velocity of 6.66 m/s.

For uniform acquisition mode, GMAP algorithm [15] was used in order to filter and estimate the power and mean velocity. Figs. 17*a* and *c* show the plan position indicator (PPI) displays of the reflectivity and the Doppler velocity estimates, respectively, obtained by means of PPP without ground clutter filtering.

The regions of highest reflectivity observed in Fig. 17*a* correspond to ground clutter. For example, at a range of 25 km and an azimuth of 185° we identify the Cerro Catedral peak and at 60 km of range and an azimuth of 180° we observe the Cerro Tronador peak, they have a top elevation of 2100 and 3491 m above the sea level, respectively. There are a lower relevant mountain clusters at 25 km range and 100° azimuth, with average top elevation around 2000 m above the sea level. In the Doppler map, Fig. 17*c*, the described regions present a mean velocity of approximately zero, as expected.

Note that Fig. 17*c* presents stripes of Doppler velocities of 5.7–6.6 m/s next to stripes of Doppler velocity of −6.6 to −5.7 m/s, with abrupt transitions between stripes. This behaviour suggests the existence of aliasing as a consequence of the low value of unambiguous velocity.

On the other hand, Figs. 17*b* and *d*, also show the PPI displays of the reflectivity and the Doppler velocity estimates, respectively, but after applying the GMAP algorithm to remove ground clutter.

From a qualitative analysis of the graphics we observe in both, the reflectivity and the Doppler velocity, that the identified ground clutter was suppressed with the use of GMAP. In addition, the zones where there is no ground clutter the reflectivity and the Doppler velocity is similar with and without clutter filtering. Naturally, the aliasing effect also appears when GMAP is applied.

In order to increase the unambiguous velocity to reduce the aliasing effect and to resolve the true velocity we used the dataset collected using the staggered acquisition mode.

Analogous to the processing with uniform-PRT, we estimate the reflectivity and the Doppler velocity in two situations: using and without using a ground clutter filter. In this case, we applied the proposed ASPASS.

Figs. 18*a* and *c* show the PPI displays of the reflectivity and of the Doppler velocity, respectively, obtained without ground clutter filtering and by means of DA for the velocity. Note that, while there are small intensity differences, there is a correspondence between Fig. 18*a* and Fig. 17*a* regarding clutter and meteorological target regions.

On the other hand, great differences can be observed between Fig. 18*b* and Fig. 17*b*. The Doppler velocity map in the second one does not have the abrupt velocity transition stripes, as expected. With staggered-PRT processing the radial velocity changes gradually, and the aliansing effect is not appreciated. This behaviour can be interpreted as the storm moving above the radar in, approximately, northwest-southeast direction. There are only two small regions located after 50 km of range for azimuth of 10°

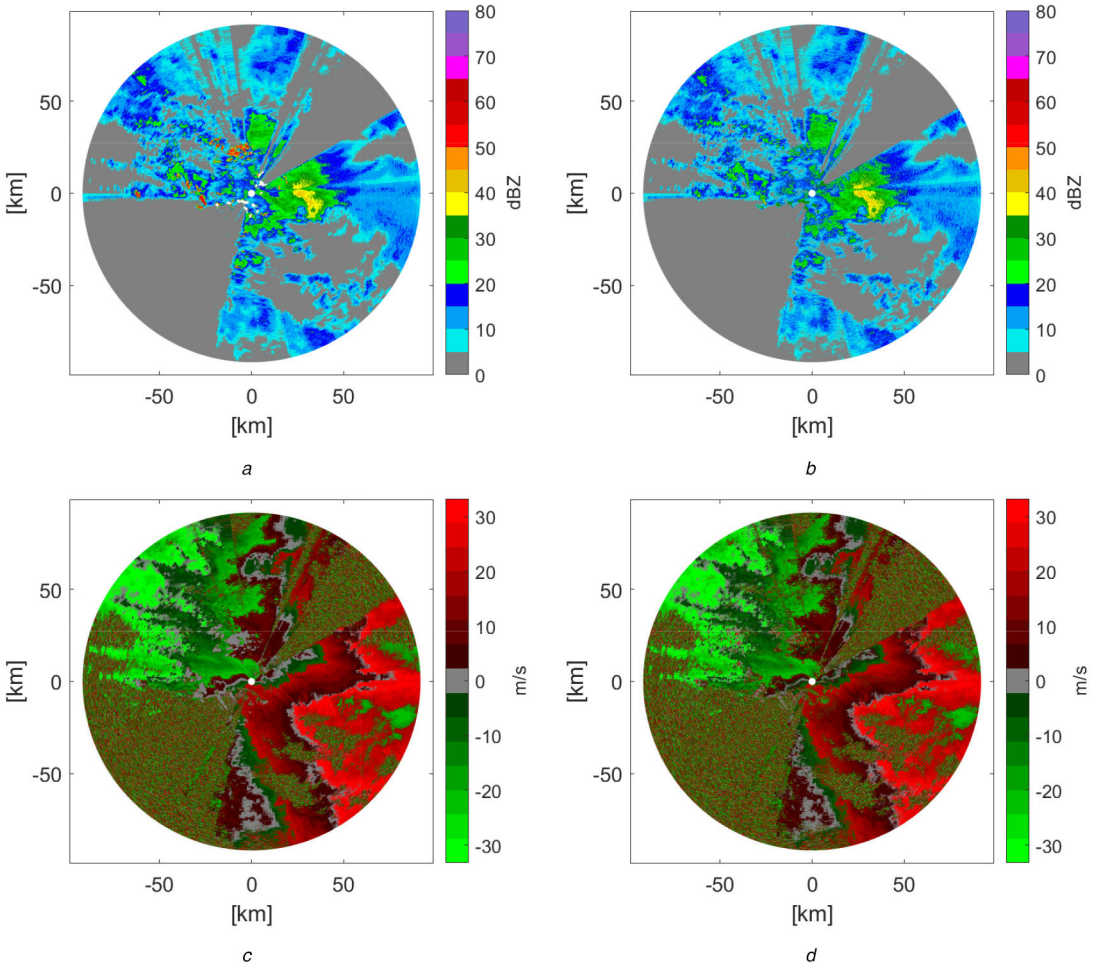

Fig. 18 *PPI plots show the performance of DA and ASPASS on RMA-12 measurements*
(a) Reflectivity from data collected with RMA-12, ***(b)*** Reflectivity obtained after ASPASS processing, ***(c)*** Velocity before ground clutter filter using DA, ***(d)*** Velocity using ASPASS

and $-20°$, approximately, where the aliasing effect persists as the unambiguous velocity of 33.25 m/s is not yet large enough for the storm's radial velocity.

In addition, Figs. 18*b* and *d* show the PPI displays of the reflectivity and the Doppler velocity estimates, respectively, after applying ASPASS, using a Kaiser window with $\alpha = 8$, to remove ground clutter. In Fig. 18*b*, it can be clearly observed that the ground clutter regions that we identified were removed by ASPASS. From both figures Figs. 18*b* and *d* note, also, that the reflectivity and the Doppler velocity are reconstructed after applying ASPASS. Finally, comparing Figs. 18*c* and *d* we observe that ASPASS also reduces the aliasing effect. The zero Doppler velocity stripes that persist in the velocity PPI display of Fig. 18*d* is due to storm zero velocity.

5 Conclusion

We proposed a novel spectral algorithm for ground clutter filtering and meteorological target spectral moments estimation in weather radar with staggered-PRT. It can be considered an extension of the GMAP algorithm for non-uniform-PRT. ASPASS is based on the fact that after zero interpolation of the staggered data sequence the resulting spectrum has five replicas and each one is assumed Gaussian-shaped. Then, the ground clutter is removed using a clutter mask built considering five Gaussian replicas. Given its mathematical complexity, we evaluated the amplitude ratio between replicas by means of numerical simulations.

Due to the problem particularities the spectral moments estimators were also modified with respect to their classical versions in order to get the power, the Doppler velocity and the spectrum width, obtaining expressions for each estimator.

We evaluated the bias and the standard deviation of the spectral moments estimates by means of Monte Carlo simulations using synthetic data in different signal composition situations. Comparison against GMAP-TD was performed, showing comparable results for both algorithms, and that in average ASPASS gets better estimates for weather spectral widths above 2 m/s. In terms of complexity, GMAP-TD takes a five-fold higher computation time than ASPASS. The study varying the CSR shows that ASPASS perform well even for large CSR values.

We also compared the performance of the ASPASS algorithm using a staggered-PRT sweep of real radar data with the GMAP algorithm using a uniform-PRT sweep of real radar data recorded with a difference of 5 min, under the same meteorological conditions. We identified ground clutter regions based on the knowledge of the terrain where the radar is located. The analysis shows that ASPASS and GMAP are able to remove the ground clutter. However, the uniform-PRT processing presents aliasing due to the low value of the unambiguous velocity. Instead, the staggered-PRT processing reduces the aliasing.

Finally, ASPASS shows a good performance, similar to the performance of other ground clutter filters of its kind. However, analogous to GMAP, ASPASS has the advantage of a low computational load as a consequence of its spectrum domain operation, making it attractive for real time applications. A possible next step is to extend the ASPASS approach to also evaluate polarimetric variables (i.e. differential reflectivity, differential phase, and correlation coefficient) for dual-polarised staggered PRT data in alternating modes [29, 30]. Including polarimetric information would also allow to increase by a factor of 2 the unambiguous velocity interval with the proper procedure to resolve the ambiguity [1].

6 Acknowledgments

This work was supported by the Universidad Nacional de Cuyo C038 4142/19, the Fondo para la Investigación Científica y Tecnológica PICT-2018-01277, the Consejo Nacional de

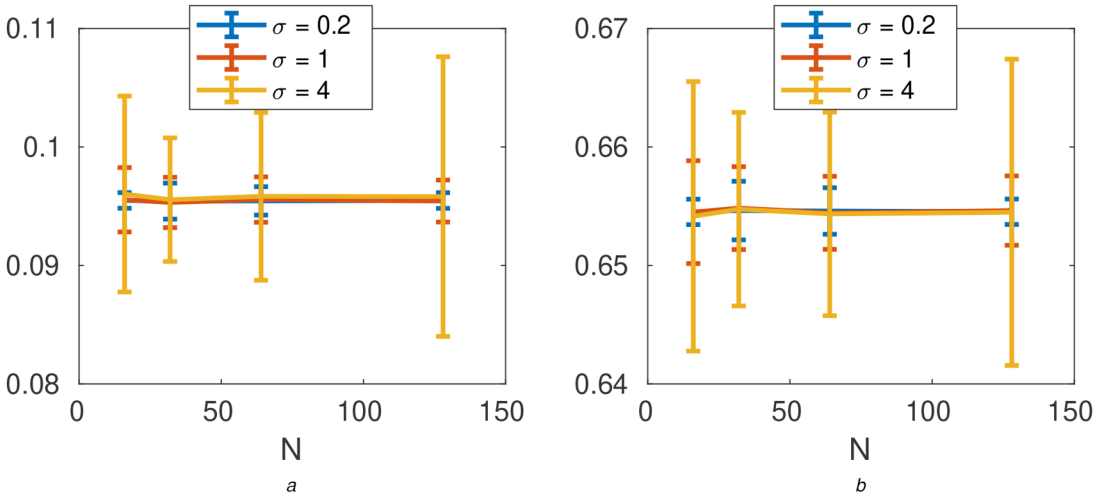

Fig. 19 *Ratios of replicas amplitudes respect the main replica*
(a) $S(0.4v_{max})/S(0)$, ***(b)*** $S(0.8v_{max})/S(0)$. The window used was a Kaiser with $\alpha = 8$

Investigaciones Científicas y Técnicas and the Comisión Nacional de Energía Atómica. RMA data was provided by Secretaría de Infraestructura y Política Hídrica, Ministerio del Interior, Obras Públicas y Vivienda of the Argentinean National Government framed within the SINARAME Project. The National System of Weather Radars (Sistema Nacional de Radares Meteorológicos, SINARAME) project was an Argentinean effort to expand the radar network over the whole country.

7 References

[1] Doviak, R.J., Zrnić, D.S.: '*Doppler radar and weather observations*' (Dover, 2014)
Q2 [2] Zrinc, D., Mahapatra, P.: 'Two methods of ambiguity resolution in pulse Doppler weather radars', *IEEE Trans. Aerosp. Electron. Syst.*, 1985, **AES-21**, (4), pp. 470–483
[3] Tahanout, M., Adane, A.E.H., Parent du Châtelet, J.: 'An improved M-PRT technique for spectral analysis of weather radar observations', *IEEE Trans. Geosci. Remote Sens.*, 2015, **53**, (10), pp. 5572–5582
[4] Sachidananda, M., Zrnić, D.: 'Clutter filtering and spectral moment estimation for Doppler weather radars using staggered pulse repetition time (PRT)', *J. Atmos. Oceanic Technol.*, 2000, **17**, (3), pp. 323–331
[5] Groginsky, H.L., Glover, K.M.: 'Weather radar canceller design'. 19th Conf. on Radar Meteorology, Miami Beach, Fl, 1980, pp. 192–198
[6] Banjanin, Z.B., Zrnic, D.S.: 'Clutter rejection for Doppler weather radars which use staggered pulses', *IEEE Trans. Geosci. Remote Sens.*, 1991, **29**, (4), pp. 610–620
[7] Bachmann, S.M.: 'Using the existing spectral clutter filter with the nonuniformly spaced time series data in weather radar', *IEEE Geosci. Remote Sens. Lett.*, 2008, **5**, (3), pp. 400–403
[8] Meymaris, G., Hubbert, J., Dixon, M.: 'Alternative approaches to staggered PRT clutter filtering'. 34th Conf. on Radar Meteorology. P5.21, Williamsburg, VA, 2009
[9] Rosell, A.C., Areta, J., Pascual, J.P.: 'Ground clutter filtering for weather radar using staggered pulse repetition time'. 2018 Argentinian Biennial Congress (ARGENCON), San Miguel de Tucumán, 2018, pp. 1–6
[10] Sachidananda, M., Zrnic, D.: 'An improved clutter filtering and spectral moment estimation algorithm for staggered PRT sequences', *J. Atmos. Oceanic Technol.*, 2002, **19**, (12), pp. 2009–2019
[11] Torres, S., Bachmann, S., Zrnic, D.: 'Signal design and processing techniques for WSR-88D ambiguity resolution – part 11: staggered PRT and updates to SZ-2 algorithm', NOAA, National Severe Storms Laboratory, Norman, OK, 2007
[12] Moisseev, D.N., Nguyen, C.M., Chandrasekar, V.: 'Clutter suppression for staggered PRT waveforms', *J. Atmos. Oceanic Technol.*, 2008, **25**, (12), pp. 2209–2218
[13] Nguyen, C.M., Chandrasekar, V.: 'Gaussian model adaptive processing in time domain (GMAP-TD) for weather radars', *J. Atmos. Oceanic Technol.*, 2013, **30**, pp. 2571–2584
[14] Warde, D.A., Torres, S.M.: 'The autocorrelation spectral density for Doppler-weather-radar signal analysis', *IEEE Trans. Geosci. Remote Sens.*, 2013, **52**, (1), pp. 508–518
[15] Siggia, A.D., Passarelli, R.E.: 'Gaussian model adaptive processing (GMAP) for improved ground clutter cancellation and moment calculation'. Proc. 3erd ERAD, 2004, pp. 67–73
Q3 [16] Torres, S.M., Warde, D.A.: 'Ground clutter mitigation for weather radars using the autocorrelation spectral density', *J. Atmos. Oceanic Technol.*, 2014, **31**, (10), pp. 2049–2066
[17] Hubbert, J.C., Dixon, M., Ellis, S.M.: 'Weather radar ground clutter. Part II: real-time identification and filtering', *J. Atmos. Oceanic Technol.*, 2009, **26**, pp. 1181–1197
[18] Ice, R.L., Rhoton, R.D., Krause, J.C., *et al.*: 'Automatic clutter mitigation in the WSR-88D, design, evaluation, and implementation'. 34th Conf. Radar Meteorology. P5.3, Williamsburg, VA, 2009
[19] Jenq, Y.C.: 'Perfect reconstruction of digital spectrum from nonuniformly sampled signals', *IEEE Trans. Instrum. Meas.*, 1997, **46**, (3), pp. 649–652
[20] Torres, S., S, M., Zrnic, D.: 'Signal design and processing techniques for WSR-88D ambiguity resolution – part 9: phase coding and staggered PRT', NOAA, National Severe Storms Laboratory, Norman, OK, 2005
[21] Fang, M., Doviak, R.J., Melnikov, V.: 'Spectrum width measured by WSR-88D: error sources and statistics of various weather phenomena', *J. Atmos. Oceanic Technol.*, 2004, **21**, (6), pp. 888–904
[22] Warde, D.A., Torres, S.M.: 'Automatic detection and removal of ground clutter contamination on weather radars'. 34th Conf. on Radar Meteorology, P10.11, Williamsburg, VA, 2009
[23] Hubbert, J.C., Dixon, M., Ellis, S.M.: 'Weather radar ground clutter. Part I: identification, modeling, and simulation', *J. Atmos. Oceanic Technol.*, 2009, **26**, pp. 1165–1180
[24] Welch, D.P.: 'The use of fast Fourier transform for the estimation of power spectra: a method based on time averaging over short, modified periodograms', *IEEE Trans. Audio Electroacoust.*, 1967, **AU-15**, pp. 70–73
[25] Torres, S.: 'Range and velocity ambiguity mitigation on the WSR-88D: performance of the staggered PRT algorithm'. 22nd Int. Conf. on Interactive Information and Processing Systems for Meteorology, Oceanography and Hydrology 9.9, Atlanta, GA, 2006
[26] Porat, B.: '*A course in digital signal processing*' (John Wiley & Sons, Inc., 1997)
[27] Zrnić, D.S.: 'Simulation of weather like Doppler spectra and signals', *J. Appl. Meteor.*, 1975, **14**, (4), pp. 619–620
[28] Rosell, A.C., Pascual, J.P., Areta, J.: 'Spectrum width correction for clutter mitigation in weather radar'. 2019 XVIII Workshop on Information Processing and Control (RPIC), Bahía Blanca, 2019, pp. 135–139
[29] Sachidananda, M., Zrnic, D.: 'Ground clutter filtering dual-polarized, staggered PRT sequences', *J. Atmos. Oceanic Technol.*, 2006, **23**, pp. 1114–1130
[30] Nguyen, C.M., Chandrasekar, V.: 'Polarimetric variables retrieval with clutter suppression for staggered PRT sequences', *J. Atmos. Oceanic Technol.*, 2015, **32**, pp. 767–782

8 Appendix

8.1 Calculation of Gaussian amplitudes

In 2/3 staggered acquisition mode, after zero interpolation of time signal, five replicas of the original clutter and precipitation PSD are present [13]. In this section, the amplitudes of the replicas with respect to the main replica are studied. Due to the problem complexity, we have not found an analytic expression for the interpolated PSD. Instead we used Monte Carlo simulations to estimate the ratios $\mathrm{PSD}(0.4v_{max})/\mathrm{PSD}(0)$ and $\mathrm{PSD}(0.8v_{max})/\mathrm{PSD}(0)$. Different number of samples and spectrum widths were considered. The simulation parameters are like in Table 2, except for $\sigma = [0.2, 1, 4]$ m/s and $N = [16, 32, 64, 128]$. 1000 Monte Carlo realisation were used for each σ and N. Fig. 19*a* shows the mean value of the ratio $\mathrm{PSD}(0.4v_{max})/\mathrm{PSD}(0)$, the error bar corresponds to the standard deviation. Fig. 19*b* shows the mean value of the ratio $\mathrm{PSD}(0.8v_{max})/\mathrm{PSD}(0)$, the error bar corresponds to the standard deviation. For this study, a Kaiser window was used with

$\alpha = 8$. From last figure, and similar studies using other windows, we consider that reasonable approximate values for the amplitude replicas are 0.095 and 0.655 respect to the main replica. The exact values of this ratio are not relevant as ASPASS is not sensible to them.

Author Queries

Q Please make sure the supplied images are correct for both online (colour) and print (black and white). If changes are required please supply corrected source files along with any other corrections needed for the paper.
Q1 Please confirm the changes made in the article title.
Q2 Please provide the location of the publisher (country) in Refs. [1, 26].
Q3 Please provide place of conference in Ref. [15].